LEED structure determination of tetragonal MnNi films on Ni(100)

M. Wuttig and C. C. Knight
Institut für Grenzflächenforschung und Vakuumphysik, Forschungszentrum Jülich, Postfach 1913, 52425 Jülich, Federal Republic of Germany
(Received 1 December 1992)

The structure of compositionally ordered MnNi films epitaxially grown on Ni(100) by deposition of 3–4 monolayers Mn above 550 K is characterized. Using a quantitative low-energy-electron-diffraction (LEED) intensity analysis, the first two interlayer spacings have been determined to be $d_{12}=1.76\pm0.02$ and $d_{23}=1.86\pm0.03$ Å. Third and deeper interlayer spacings of 1.87 ± 0.04 and 1.88 ± 0.04 Å, respectively, have been found. A pronounced corrugation is observed for the first layer only, where the Mn atoms are displaced outwards by 0.30 ± 0.02 Å. This surface layer has a composition of 50% Mn and 50% Ni. Deeper layers have a similar composition, but due to the relative insensitivity to the composition in deeper layers other concentrations cannot be excluded by the LEED analysis. The resulting film structure is indicative of the formation of tetragonal MnNi films.

I. INTRODUCTION

In recent years, low-energy electron diffraction (LEED) has been successfully used to study the composition and structure of the surfaces of disordered bulk alloys.[1–4] These studies have significantly contributed to our understanding of the segregation at alloy surfaces. Highlights of these investigations include the observation of an oscillatory segregation profile in the near-surface region[1,3] and a strong dependence of the segregation profile on the surface orientation.[2] Basically all of these studies have concentrated on the investigation of alloys where the relatively large difference in the atomic number of the constituting elements made possible an accurate determination of the composition in the near-surface region. Here we want to report on our structural analysis of MnNi alloy films formed by deposition of Mn on Ni(100). In this case, the small difference in atomic numbers leads to relatively similar phase shifts. This in turn puts severe constraints on the precise determination of the film composition. Nevertheless, it was possible to determine the structure and composition of the films.

In a previous publication, the growth of manganese on Ni(100) and the resulting superstructures have been reported.[5] While deposition of Mn below 270 K leads to the formation of Mn films on the Ni(100) surface, incorporation and alloy formation are observed for deposition temperatures above 270 K. Upon deposition of 0.5-ML (monolayer) Mn at temperatures between 300 and 500 K, an ordered surface alloy with $c(2\times2)$ structure is formed. Here 1 ML (monolayer) is defined with respect to the atomic density of the Ni(100) surface, i.e., it corresponds to an atomic concentration of 1.61×10^{15} atoms/cm^2. Using a full dynamical LEED analysis the structure of this surface was determined.[6] The first layer consists of an ordered alloy (surface alloy) where the Mn atoms are displaced outwards by 0.25 ± 0.02 Å. The resulting corrugation is responsible for intense $c(2\times2)$ superstructure beams.[6] Similar $c(2\times2)$ structures, albeit with smaller corrugation, have been produced by the deposition of 0.5-ML Au (Refs. 7–9) and Pd (Refs. 10 and 11) on Cu(100) at growth temperatures above 270 K. In none of these cases, however, was it possible to grow thicker ordered alloy films.

In contrast to the behavior found for these surface alloys, it is possible to grow thicker ordered alloy films on Ni(100). This has been shown by MEED (medium-energy-electron-diffraction) and LEED (low-energy-electron-diffraction) experiments where films with $c(2\times2)$ structure were even found after deposition of 4-ML Mn.[5] In these experiments, changes in structure and morphology at different growth temperatures were found after deposition of multiples of 0.5-ML Mn.[5] For the 4-ML-thick alloy film, the Auger intensity of the Mn transition at 589 eV and the Ni transition at 848 eV was measured in the first derivative mode with a cylindrical mirror analyzer using a primary energy of 3 keV. The intensity ratio of these transitions has been determined to $I_{Mn}/I_{Ni}=0.92\pm0.08$. Using the known sensitivity of these two Auger transitions of 0.88,[12] a composition of approximately 50% Mn and 50% Ni is obtained for the bulk alloy film. These results suggest that each of the growing alloy layers has a manganese concentration of 50%. Thus deposition of 4-ML Mn should produce an alloy film eight layers thick. Here we want to present the results of our structural analysis for these thicker alloy films ("bulk alloys") which have been produced by deposition of Mn on Ni(100) at elevated temperatures.

The paper is organized in the following manner. The experimental setup will be described in Sec. II. Details of the LEED calculations and the results of the LEED analysis are given Sec. IV. In Sec. IV, the results are discussed and compared with similar experimental systems.

II. EXPERIMENT

The experiments were performed in an UHV (ultrahigh vacuum) chamber with a base pressure of 5×10^{-9} Pa.

0163-1829/93/48(16)/12130(6)/$06.00

During Mn evaporation the pressure never exceeded 2×10^{-8} Pa. After deposition the Mn source was turned off and the pressure quickly dropped to the base pressure. The evaporation rate was determined by a quartz-crystal microbalance. This enabled a precise determination of the film thickness. Further confirmation of the film thickness came from the measurement of MEED or LEED intensities during Mn deposition. These intensities show maxima and minima at certain well-defined coverages which allow a careful control of the film thickness. This has been discussed in detail in Ref. 5, where the apparatus and our sample treatment have already been described. Therefore we will focus here only on the experimental details relevant for the LEED *I-V* measurements.

The intensities of up to eight different beams were measured simultaneously by a video LEED system.[13] Data were recorded in steps of 0.5 eV for six nonequivalent beams [(1,0), (1,1), (2,0), (2,1), $(\frac{1}{2},\frac{1}{2})$, and $(\frac{3}{2},\frac{1}{2})$] from 40 to around 350 eV at normal incidence. To approach perfect alignment of the system, magnetic fields were strongly reduced by double mu-metal shielding of the entire UHV chamber. Normal incidence was defined as the angle where symmetry-equivalent beams were as similar as possible. Tilt and polar angles were varied until these beams had almost identical curves (Pendry R factor $R_p<0.05$, typically $R_p\simeq0.03$), showing that normal incidence was closely approached. After an automatic background subtraction, symmetry-equivalent beams were averaged and normalized to a constant incident current. The whole data set had an energy range of approximately 1400 eV.

In Fig. 1, the *I-V* curves for the $c(2\times2)$ structure formed after deposition of 4-ML Mn at 600 K are shown. To increase the structural order in the films, the sample was annealed for five additional minutes at 600 K after deposition. This leads to sharp and intense $c(2\times2)$ superstructure beams and low background intensity. Then the sample was cooled to 150 K, and *I-V* curves were measured at this temperature. This structure was prepared three times *ex nuovo* and practically identical *I-V* curves were obtained. Additionally, the influence of film thickness and deposition temperature on the *I-V* curves was checked. For films between 3- and 4-ML Mn, the *I-V* curves are basically indistinguishable provided that the deposition temperature was above 550 K. In general, the background was lower at higher growth temperatures, but the *I-V* curves did not change. By contrast, the *I-V* curves obtained for the $c(2\times2)$ surface alloy formed after deposition of 0.5 ML at 425 K (shown as broken lines in Fig. 1) are rather different. This indicates that the structure of the surface alloy is considerably different from that of the bulk alloy film.

III. STRUCTURE DETERMINATION

A. LEED calculations

A LEED program developed by Moritz[14] was used for the calculation of the LEED intensities. This program uses symmetry-adapted functions to reduce the angular momentum components and employs the layer doubling method to stack the layers. The diffraction matrices for different layers were calculated by matrix inversion. A maximum of ten phase shifts derived from band-structure calculations[15] was used to describe the atomic scattering. They were corrected for thermal diffuse scattering using a Debye temperature of 440 and 435 K for Mn and Ni, respectively. To investigate the distribution of Mn over several layers or the partial occupation of different sublattices, the averaged-t-matrix approximation (ATA) was used. In this approximation each layer or sublattice is occupied by an "averaged atom." The energy-dependent refractive potential $V_0(E)$ and the absorptive potential $V_i(E)$ were those previously used for Ni,[16] and were assumed to be identical for all layers. As is typically done, the final value for the real part of the inner potential was adjusted within the theory-experiment fitting procedure. This fit was performed using three different R factors, the Pendry R factor (R_P),[17] the Zanazzi-Jona R factor (R_{ZJ}),[18] and the R_{DE} R factor.[19] The latter evaluates the deviation between the normalized experimental and theoretical intensity spectra. Estimates of the error bar

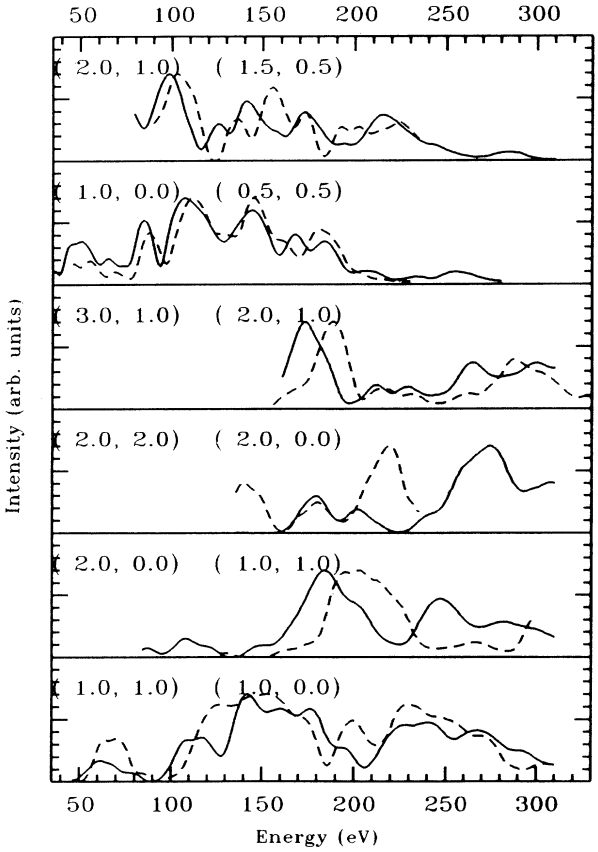

FIG. 1. Experimental spectra obtained after deposition of 4-ML Mn at 600 K (solid line) and after deposition of 0.5-ML Mn at 400 K (broken line). Identical beams are compared and are labeled using two different notations. The beam labeling on the left-hand side is for the unit cell as shown in Fig. 2(a), while the notation on the right side is for the primitive unit cell of the Ni(100) surface.

in the structure determination are derived from the variance of R, $\mathrm{var}(R_p)=R_p\sqrt{8V_i/\Delta E}$, where ΔE is the range of energies where calculated and measured spectra overlap.

B. Structural analysis

The theoretical I-V curves calculated for the model depicted in Fig. 2 were compared to the measured I-V curves. The structure shown in Fig. 2 is characterized by an ordered arrangement of Mn and Ni atoms in which each layer has a Mn concentration of 50%. This is in agreement with the composition derived from the Auger and MEED breakpoints.[5] The atomic corrugation at the surface, the first three interlayer distances at the surface d_{12}, d_{23}, and d_{34}, and the bulk interlayer distance d_b were varied to determine the best-fit structure. The interlayer distances were varied between 1.5 and 2.1 Å in steps of 0.1 Å, and the corrugation of the first two layers was varied between -0.5 and 0.5 Å in steps of 0.1 Å. It was assumed throughout the calculations that the films grew epitaxially on the Ni(100) substrate. This is supported by the observation that the position of the integer order beams did not vary with increasing film thickness. As a consequence, the MnNi films have the in-plane lattice constant of 3.52 Å characteristic of the Ni(100) surface. After the optimum structure was determined on this rough grid, the search was continued on a finer grid where a step width of 0.01 or 0.02 Å was used. Table I shows the optimum structure obtained for the three different R factors (R_P, R_{ZI}, and R_{DE}). The variations in the best-fit structure for the different R factors are rather small and the values for the R-factor minima are quite low, indicating a satisfactory agreement between theory and experiment. This is confirmed by a visual inspection of the theoretical I-V curves obtained for the optimum structure, and the experimental spectra shown in Fig. 3. Both the peak positions and intensities of the peaks are satisfactorily described with the exception of the (2,0) beam around 180 eV. In Fig. 4, the variation of the Pendry R factor with surface corrugation and interlayer spacing is shown. This figure shows that the R-factor minima are deep, allowing a precise determination of the

TABLE I. Optimum R factors for the MnNi bulk alloy produced by deposition of 4-ML Mn on Ni(100) at 600 K. Consistent results for the different R factors are obtained.

d_{12} (Å)	d_{23} (Å)	d_{34} (Å)	d_b (Å)	Δz_1 (Å)	Δz_2 (Å)	R factor
1.76	1.86	1.87	1.88	0.30	0.00	0.327 (R_P)
1.76	1.88	1.87	1.88	0.30	0.00	0.072 (R_{ZI})
1.76	1.86	1.87	1.88	0.32	0.00	0.299 (R_{DE})

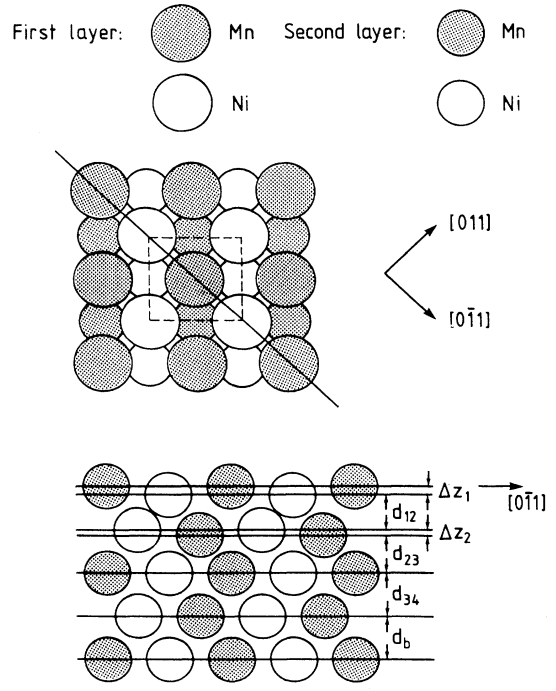

FIG. 2. Structural model for the MnNi bulk alloy. (a) Top view, where the unit cell is depicted by a broken line. The solid line denotes the cut used for the side view. (b) Side view with a definition of the structural parameters used in the LEED analysis.

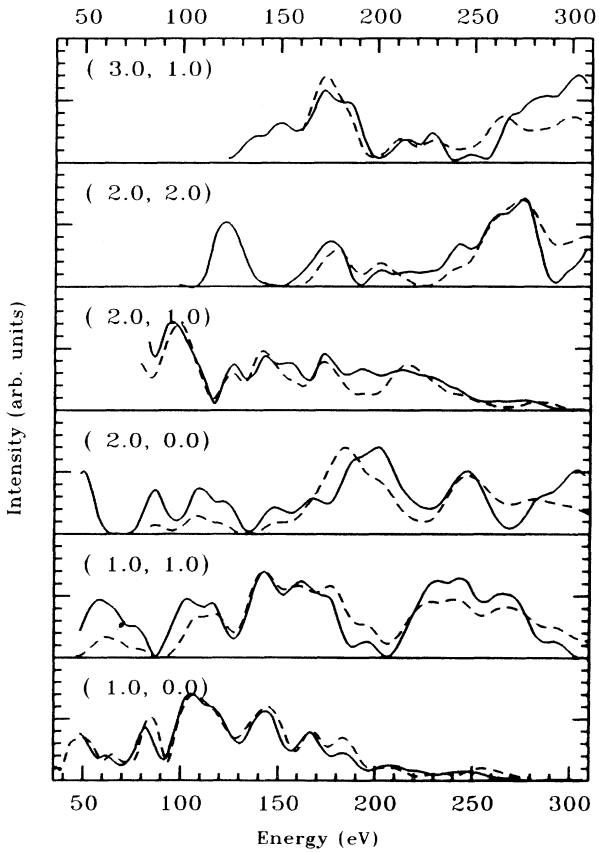

FIG. 3. Best-fit spectra for the bulk alloy (solid line) compared with the experimental spectra for the Ni(100) $c(2\times2)$Mn structure obtained after deposition of 4-ML Mn at 600 K (broken line).

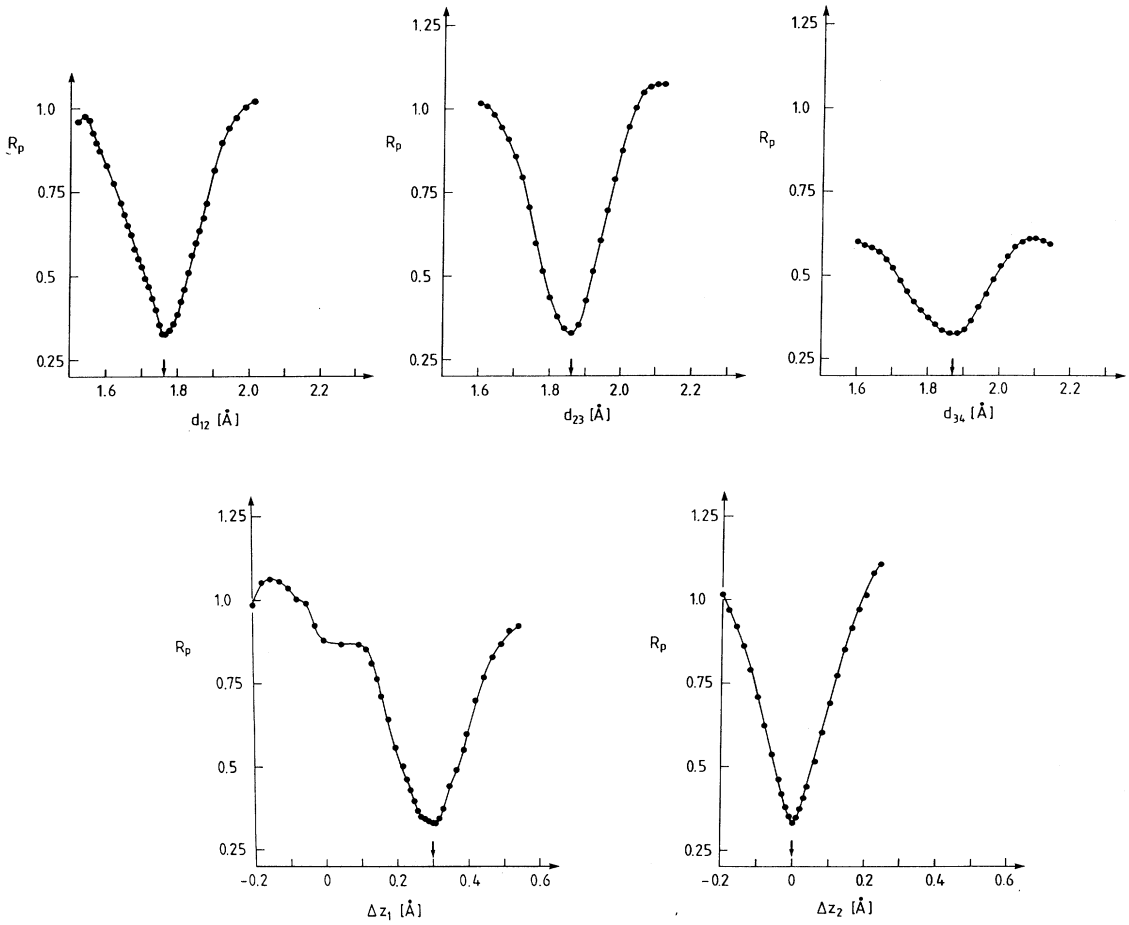

FIG. 4. Influence of a variation of different structural parameters on the theory-experiment comparison as estimated from the Pendry R factor. Shown is the variation of the first (d_{12}), second (d_{23}), and third (d_{34}) interlayer distances and the corrugation of the first (Δz_1) and the second (Δz_2) layers around the best-fit structure. Arrows show the position of the R-factor minimum. The respective values of the structural parameters are listed in the first row of Table I.

corresponding interatomic distances.

In a second stage of the structural analysis, atomic concentrations of different subplanes were varied to see if a unique solution had been found. Several different compositions were checked, and in each case the optimum structure was determined. As limiting cases, two structures were considered in which second and deeper layers contained pure Mn or pure Ni and only the first layer was composed of an ordered alloy. For these two models, the interlayer distances found after optimization were identical to the best-fit structure of the ordered bulk alloy listed in Table I. This shows that the interlayer distances found in the R-factor analysis are basically independent of the composition of deeper layers. All three R factors found for these two limiting cases (pure Ni and pure Mn in deeper layers) are worse than the three minimum R-factors for the ordered bulk alloy. Nevertheless, the variations of the R factors with composition are only of the order of 3%, which is still within the error bar of the structural analysis. For the first layer, on the other hand, the composition can be determined uniquely. Satisfactory agreement between theory and experiment is only obtained for a Mn concentration close to 50%. Basically all Mn atoms occupy one sublattice and are displaced outwards by 0.30 ± 0.02 Å. An outward displacement of Ni by the same amount leads to a considerably worse R factor ($R_P=0.46$) after optimizing the other interlayer distances.

IV. DISCUSSION

The structural analysis shows that upon deposition of 3–4-ML Mn on Ni(100) at elevated temperatures, a film with the structure as listed in Table I is obtained. An ordered alloy is found for the surface plane, in which Mn atoms are displaced outside by 0.30 ± 0.02 Å. For deeper layers, a composition of 50% Mn and 50% Ni for each plane is favored, but other concentrations cannot be excluded. On the other hand, the interlayer distances can be uniquely determined independent of the composition of the deeper layers. This is in agreement with LEED studies by Gauthier and co-workers,[1–3] who found that

for different disordered PtNi, PtFe, and PtCo alloys the composition and the interlayer distances in the surface region could be optimized independently of each other. Similar to our findings, they observed that the dependence of the R factor on interlayer distances is more pronounced than on the composition. These conclusions are supported by the structural analysis obtained for MoRe alloys.[4] In the studies mentioned above, the relatively large difference in the atomic number of the constituting elements of the alloys enabled a determination of the composition profile in the near-surface region. For the alloy studied here, the phase shifts of Mn and Ni are quite similar since the atomic number of the elements only differs by 3. Therefore it is difficult to determine uniquely the composition of deeper layers for the MnNi alloy films. In order to characterize the composition of the films, a different approach had to be chosen. Fortunately, the interlayer distances for the MnNi films which are summarized in the first row of Table II are rather different from both the clean Ni(100) surface and the $c(2\times2)$ structure obtained after deposition of 0.5-ML Mn on Ni(100). These interlayer distances can thus be used as a fingerprint of the structure that was formed. The question was therefore which MnNi alloys have interlayer distances close to the values observed in this analysis and which can also account for the observed LEED pattern.

In the bulk phase diagram, a variety of alloy phases exists.[20] Disordered alloys are observed above 900 K. Since the alloy films in this study were stable at much lower temperatures, disordered MnNi films were excluded. In the bulk phase diagram there are three ordered alloys which could possibly account for the $c(2\times2)$ structure and the observed interlayer spacings. These are the tetragonal and the cubic phases of MnNi and the cubic phase of $MnNi_3$.[21] The cubic phase of MnNi has a CsCl structure with a lattice constant of 2.98 Å.[21] Only an unreasonably high strain would allow this structure to match the in-plane lattice constant of 3.52 Å of the Ni(100) surface. Therefore this phase can be excluded. $MnNi_3$ has a Cu_3Au structure with a lattice spacing of 3.589 Å.[21] This produces a misfit of 2%. As a consequence, the critical thickness for the dislocation formation should be approximately 8 Å.[22] Contrary to this scenario expected for the formation of cubic $MnNi_3$, no evidence for misfit dislocation was found for films up to 15 Å thick. Additionally, one would expect an expansion of the interlayer distance to 1.93 Å due to the misfit-induced strain. This distance, however, is larger than the observed bulk interlayer spacing of the film. The final possibility is the tetragonal phase of MnNi. This structure has a bulk lattice constant of 3.53 Å in the plane and 3.72 Å in the normal direction.[21] Therefore the misfit between the MnNi(100) films and the Ni(100) surface is only 0.1%. The resulting interlayer spacing of 1.87 Å is in excellent agreement with the observed interlayer distance of 1.88 Å. This observed structure thus agrees very well with a slightly strained tetragonal MnNi film. Each alloy layer has a Mn concentration of 50%, in agreement with Auger and MEED data.[5] The tetragonal MnNi phase is the most stable bulk phase of all Mn_xNi_{1-x} alloys, i.e., it has the highest heat of formation.[20] This stability together with the small misfit to the Ni(100) surface can explain why it was not possible to grow other Mn_xNi_{1-x} alloy phases on Ni(100).

Finally, it is worthwhile to address the surface structure of the tetragonal MnNi film on Ni(100). While the second and third interlayer spacings are close to the bulk value, the first interlayer spacing is considerably smaller. As can be seen from the definition of the parameters in Fig. 2, this number describes the distance from the second layer to the lower-lying Ni atom in the first layer. The Mn atoms, on the other hand, are displaced outwards by 0.3 Å. This leads to an average interlayer spacing of 1.92 Å, which is similar to the bulk interlayer spacing of the film. It is interesting to speculate on the origin of this strong corrugation of the MnNi film. We believe that this corrugation should be closely related with the magnetic properties of the film surface. It has been recently shown[23] that the strong corrugation of 0.30 ± 0.02 Å found for the Cu(100) $c(2\times2)$Mn surface alloy formed after deposition of 0.5-ML Mn (Ref. 6) is due to the enhanced magnetic moment of the Mn atom. A similar behavior is also expected for the surface and bulk alloys formed upon Mn deposition on Ni(100). It seems worthwhile to corroborate this effect by total-energy calculations and to look for surface magnetism experimentally.

TABLE II. Best-fit structure from the LEED analyses of the Ni(100) surface (Ref. 24), the surface alloy formed upon deposition of 0.5-ML Mn on Ni(100) (Ref. 6), and the bulk alloy produced by deposition of 4-ML Mn on Ni(100) (this work). The error bars have been determined from the variation of the Pendry R factor. For comparison the expected structure of tetragonal MnNi(100) films epitaxially grown on Ni(100) is listed. The in-plane lattice constant is denoted by a.

Structure	Ni(100)	Ni(100) $c(2\times2)$Mn 0.5-ML Mn	Ni(100) $c(2\times2)$Mn 4-ML Mn	Tetragonal MnNi on Ni(100)
Δz_1 (Å)		0.25±0.02	0.30±0.02	
Δz_2 (Å)		0.00±0.03	0.00±0.03	
d_{12} (Å)	1.74±0.02	1.76±0.02	1.76±0.02	
d_{23} (Å)	1.76	1.78±0.03	1.88±0.03	
d_{34} (Å)	1.76	1.75±0.04	1.87±0.04	
d_b (Å)	1.76	1.76	1.88±0.04	1.87
a (Å)	3.52	3.52	3.52	3.52

V. SUMMARY

The structure and composition of MnNi films epitaxially grown on Ni(100) has been determined using a quantitative LEED intensity analysis. Even though the relatively weak difference in the atomic phase shifts of Mn and Ni impedes a unique determination of the composition profile of deeper film layers, the interlayer distances determined can be successfully used as a fingerprint of the resulting film composition. The large expansion of the interlayer distances to around 1.87 Å is characteristic of the formation of tetragonal MnNi films which grow with marginal misfit (0.1%) on Ni(100). In these films each layer ideally has a composition of 50% Mn and 50% Ni. This composition is favored by the LEED analysis, although other compositions cannot be excluded. Furthermore, this composition is supported by our study of the film growth by MEED, LEED and Auger.[5] At the MnNi film surface, a pronounced corrugation of 0.30 ± 0.02 Å is observed. This corrugation is possibly linked with the magnetic properties of the surface, as has been shown for the Cu(100) $c(2\times2)$Mn surface alloy.

ACKNOWLEDGMENTS

One of us (C.C.K.) thanks the Alexander von Humboldt-Stiftung for financial support. Financial support by the "Fonds der Chemischen Industrie" is gratefully acknowledged. In addition we thank Y. Gauthier, S. Blügel, and H. Over for helpful discussions, and J. Larscheid for his technical assistance. We gratefully acknowledge the help of W. Moritz for making available his LEED code. This work is part of the scientific program on "Alloy surfaces" conducted by the European Science Foundation (ESF), within the Surface Crystallography Network.

[1]Y. Gauthier and R. Baudoing, in *Segregation and Related Phenomena,* edited by P. Dowben and A. Miller (CRC, Boca Raton, FL, 1990).

[2]Y. Gauthier, R. Baudoing, M. Lundberg, and J. Rundgren, Phys. Rev. B **35**, 7867 (1987).

[3]Y. Gauthier, R. Baudoing-Savois, J. M. Bugnard, U. Bardi, and A. Atrei, Surf. Sci. **276**, 1 (1992), and references therein.

[4]B. Dötsch, A. Schmidt, L. Hammer, N. Kottcke, R. Döll, K. Heinz, K. Müller, H. L. Davis, and D. M. Zehner (unpublished).

[5]M. Wuttig, T. Flores, and C. C. Knight, Phys. Rev. B **48**, 12 082 (1993).

[6]M. Wuttig, C. C. Knight, T. Flores, and Y. Gauthier, Surf. Sci. **292**, 189 (1993).

[7]P. W. Palmberg and T. N. Rhodin, J. Chem. Phys. **49**, 134 (1968).

[8]Z. Q. Wang, Y. S. Li, C. K. C. Lok, J. Quinn, and F. Jona, Solid State Commun. **62**, 181 (1987).

[9]D. D. Chambliss and S. Chiang, Surf. Sci. **264**, L187 (1992).

[10]S. C. Wu, S. H. Lu, Z. Q. Wang, C. K. C. Lok, J. Quinn, Y. S. Li, D. Tian, and F. Jona, Phys. Rev. B **38**, 5363 (1988).

[11]T. D. Pope, G. W. Anderson, K. Griffiths, and P. R. Norton, Phys. Rev. B **44**, 11 518 (1991).

[12]*Handbook of Auger Electron Spectroscopy* (Physical Electronics, Eden Prarie, MI, 1972).

[13]K. Heinz, Prog. Surf. Sci. **27**, 239 (1988).

[14]W. Moritz, J. Phys. C **17**, 353 (1984).

[15]V. L. Moruzzi, J. F. Janak, and A. R. Williams, *Calculated Electronic Properties of Metals* (Plenum, New York, 1978).

[16]Y. Gauthier, W. Hoffmann, and M. Wuttig, Surf. Sci. **233**, 239 (1990).

[17]J. B. Pendry, J. Phys. C **13**, 937 (1980).

[18]E. Zanazzi and F. Jona, Surf. Sci. **62**, 61 (1977).

[19]G. Kleinle, W. Moritz, and G. Ertl, Surf. Sci. **238**, 119 (1990).

[20]*Selected Values of the Thermodynamic Properties of Binary Alloys* (American Society of Metals, Metals Park, OH, 1986).

[21]*Structure Data of Elements and Intermetallic Phases,* edited by K. H. Hellwege, Landolt-Börnstein, New Series, Group III, Vol. 6, Pt. 4 (Springer-Verlag, New York, 1971).

[22]J. W. Matthews, J. Vac. Sci. Technol. **12**, 126 (1974).

[23]M. Wuttig, Y. Gauthier, and S. Blügel, Phys. Rev. Lett. **70**, 3619 (1993).

[24]W. Oed, H. Lindner, U. Starke, K. Heinz, K. Müller, and J. B. Pendry, Surf. Sci. **224**, 179 (1989).